Proceedings of the 2000 IEEE
International Conference on Control Applications
Anchorage, Alaska, USA • September 25-27, 2000

MP6-6 5:00

Adaptive Robust Precision Motion Control of Linear Motors with Ripple Force Compensations: Theory and Experiments [1]

Li Xu Bin Yao +

School of Mechanical Engineering
Purdue University, West Lafayette, IN 47907, USA
+ Email: byao@ecn.purdue.edu

Abstract

This paper studies the high performance robust motion control of linear motors which are subjected to significant force ripple. Based on the structural property of linear motors, some simple models with unknown weights are used to approximate the force ripple as well as other reproducible nonlinearities, such as friction. The unknown weights are adjusted on-line via certain parameter adaptation law to achieve an improved model compensation. The model approximation error as well as lumped disturbance are handled via certain robust control law to achieve a guaranteed robust performance. Experimental results are obtained for the motion control of an iron core linear motor and verify the high performance of the proposed scheme.

1 Introduction

Direct drive linear motor systems gain high-speed, high-accuracy potential by eliminating mechanical transmissions. However, they also lose the advantage of using mechanical transmissions – gear reductions reduce the effect of model uncertainties. Furthermore, certain types of linear motors are subjected to significant force ripple [1]. These uncertain nonlinearities are directly transmitted to the load and have significant effects on the motion of the load.

A great deal of effort has been devoted to solving the difficulties in controlling linear motors [1]-[5]. Alter and Tsao [2] proposed an H_∞ controller to increase dynamic stiffness for linear motor driven machine tool axes. In [3], a disturbance compensation method based on disturbance observer (DOB) [6] was proposed to make linear motors robust to model uncertainties. To reduce the effect of force ripple, in [1], feedforward compensation terms, which are based on an off-line experimentally identified model, were added to a position controller. In [4], a neural-network-based feedforward controller was proposed to reduce the effect of reproducible disturbances. In [5], the idea of adaptive robust control (ARC) [7, 8] was generalized to provide a theoretic framework for the high performance motion control of linear motors.

In this paper, the proposed desired compensation ARC (DCARC) [9] will be extended to the control of an *iron* core linear motor. Compared to the *epoxy* core linear motor studied in [9], the *iron* core linear motor is subjected to significant nonlinear ripple forces. As such, effective ripple force compensation may be needed for high performance, which is the focus of the paper. As an alternative to feedforaward force ripple compensation [1] or feedback compensation using measurements of back EMF [10], one can reduce the effect of ripple forces by utilizing the particular physical structure of the ripple forces. Specifically, design models consisting of known basis functions with unknown weights are used to approximate the unknown ripple forces. On-line parameter adaptation is then utilized to reduce the effect of various parametric uncertainties while certain robust control laws are used to handle the uncompensated uncertain nonlinearities. This yields good results and does not require measurement of back EMF. Time-consuming and costly rigorous off-line identification of ripple forces is also avoided. The resulting controller achieves a guaranteed transient performance and a prescribed final tracking accuracy in the presence of both parametric uncertainties and bounded disturbance. In the presence of parametric uncertainties only, asymptotic tracking is also achieved. In addition, the proposed controller has several implementation advantages such as reducing on-line computation time, separating the robust control design from parameter adaptation process, reducing the effect of measurement noise, and having a faster adaptation process. This scheme, as well as a PID controller, are implemented and compared on an *iron* core linear motor. Comparative experimental results are presented to show the advantages of the proposed method.

2 Problem Formulation and Dynamic Models

The linear motor considered here is a current-controlled three-phase iron core motor driving a linear positioning stage supported by recirculating bearings. The mathematical model of the system is assumed to be of the form:

$$M\ddot{q} = u - F, \qquad F = F_f + F_r - F_d, \tag{1}$$

where q represents the position of the inertia load, M is the inertia of the payload plus the coil assembly, u is the input

[1] The work is supported in part by the National Science Foundation under the CAREER grant CMS-9734345 and in part by a grant from the Purdue Research Foundation

0-7803-6562-3/00$10.00©2000 IEEE

voltage, F is the lumped effect of uncertain nonlinearities such as friction F_f, ripple force F_r and external disturbance F_d. While there have been many friction models proposed [11], a simple and often adequate approach is to regard friction force as a static nonlinear function of the velocity:

$$F_f(\dot{q}) = B\dot{q} + F_{fn}(\dot{q}), \tag{2}$$

where B is the viscous friction coefficient, and F_{fn} is the nonlinear friction term which can be modeled as [11]

$$F_{fn}(\dot{q}) = -[f_c + (f_s - f_c)e^{-|\dot{q}/\dot{q}_s|^{\xi}}]\mathrm{sgn}(\dot{q}), \tag{3}$$

where f_s is the level of static friction, f_c is the level of Coulomb friction, and $\dot{q}_s$ and ξ are empirical parameters used to describe the Stribeck effect. Substituting (2) into (1) yields

$$\begin{aligned} \dot{x}_1 &= x_2, \\ M\dot{x}_2 &= u - Bx_2 - F_{fn} - F_r + \Delta, \\ y &= x_1, \end{aligned} \tag{4}$$

where $x = [x_1, x_2]^T$ represents the position and velocity, y is the output, and $\Delta \triangleq F_d$.

3 Adaptive Robust Control of Linear Motor Systems

3.1 Design Models and Assumptions

In this paper, it is assumed that the permanent magnets of the same linear motor are identical and equally spaced at a pitch of P. Thus, $F_r(x_1)$ is a periodic function with a period of P, i.e., $F_r(x_1 + P) = F_r(x_1)$, and it can be approximated quite accurately by the first several harmonics, which is denoted as $\bar{F}_r(x_1)$ and represented by [5]

$$\bar{F}_r(x_1) = A_r^T S_r(x_1) \tag{5}$$

where $A_r = [A_{r1s}, A_{r1c}, \ldots, A_{rqs}, A_{rqc}]^T \in \mathbf{R}^{2q}$ is the unknown weight, $S_r = [\sin(\frac{2\pi}{P}x_1), \cos(\frac{2\pi}{P}x_1), \ldots, \sin(\frac{2\pi q}{P}x_1), \cos(\frac{2\pi q}{P}x_1)]^T$ is the known basis shape function, and q is the numbers of harmonics used to approximate $F_r(x_1)$.

It is seen that the friction model (3) is discontinuous at $x_2 = 0$. Thus one cannot use this model for friction compensation. To by-pass this technical difficulty, a simple continuous friction model $\bar{F}_{fn} = A_f S_f(x_2)$, where the amplitude A_f is unknown and $S_f(x_2)$ is a continuous function, will be used to approximate the actual discontinuous friction model (3) for model compensation. The second equation of (4) can thus be written as:

$$M\dot{x}_2 = u - Bx_2 - A_f S_f(x_2) - A_r^T S_r(x_1) + d, \tag{6}$$

where $d = (\bar{F}_{fn} - F_{fn}) + (\bar{F}_r - F_r) + \Delta$. Define an unknown parameter set $\theta = [\theta_1, \theta_2, \theta_3, \theta_{4b}^T, \theta_5]^T \in \mathbf{R}^{4+2q}$ as $\theta_1 = M$, $\theta_2 = B$, $\theta_3 = A_f$, $\theta_{4b} = A_r \in \mathbf{R}^{2q}$ and $\theta_5 = d_n$, the nominal value of the lumped disturbances d. Equation (6) can thus be linearly parameterized in terms of θ as

$$\theta_1\dot{x}_2 = u - \theta_2 x_2 - \theta_3 S_f - \theta_{4b}^T S_r(x_1) + \theta_5 + \tilde{d}, \tag{7}$$

where $\tilde{d} = d - d_n$. For simplicity, in the following, the following notations are used: $\bullet_i$ for the i-th component of the vector $\bullet$, $\bullet_{\min}$ for the minimum value of $\bullet$, and $\bullet_{\max}$ for the maximum value of $\bullet$. The operation $<$ for two vectors is performed in terms of the corresponding elements of the vectors. The following practical assumptions are made:

Assumption 1 *The extent of the parametric uncertainties and uncertain nonlinearities are known, i.e.,*

$$\theta \in \Omega_\theta \triangleq \{\, \theta :\ \theta_{\min} < \theta < \theta_{\max} \,\} \tag{8}$$

$$\tilde{d} \in \Omega_d \triangleq \{\, \tilde{d} :\ |\tilde{d}| \le \delta_d \,\} \tag{9}$$

where $\theta_{\min} = [\theta_{1\min}, \cdots, \theta_{5\min}]^T$, $\theta_{\max} = [\theta_{1\max}, \cdots, \theta_{5\max}]^T$, *and* δ_d *are known.* ◇

Let $\hat{\theta}$ denote the estimate of θ and $\tilde{\theta}$ the estimation error (i.e., $\tilde{\theta} = \hat{\theta} - \theta$). In view of (8), the following adaptation law with discontinuous projection modification can be used

$$\dot{\hat{\theta}} = \mathrm{Proj}_{\hat{\theta}}(\Gamma\tau) \tag{10}$$

where $\Gamma > 0$ is a diagonal matrix, τ is an adaptation function to be synthesized later. The projection mapping $\mathrm{Proj}_{\hat{\theta}}(\bullet) = [\mathrm{Proj}_{\hat{\theta}_1}(\bullet_1), \cdots, \mathrm{Proj}_{\hat{\theta}_5}(\bullet_5)]^T$ is defined in [7, 12] as

$$\mathrm{Proj}_{\hat{\theta}_i}(\bullet_i) = \begin{cases} 0 & \text{if } \hat{\theta}_i = \theta_{i\max} \text{ and } \bullet_i > 0 \\ 0 & \text{if } \hat{\theta}_i = \theta_{i\min} \text{ and } \bullet_i < 0 \\ \bullet_i & \text{otherwise} \end{cases} \tag{11}$$

3.2 ARC Controller Design

Define a switching-function-like quantity as

$$p = \dot{e} + k_1 e = x_2 - x_{2eq}, \quad x_{2eq} \triangleq \dot{y}_d - k_1 e, \tag{12}$$

where $e = y - y_d(t)$ is the output tracking error, and k_1 is any positive feedback gain. If p is small or converges to zero exponentially, then the output tracking error e will be small or converge to zero exponentially since $G_p(s) = \frac{e(s)}{p(s)} = \frac{1}{s+k_1}$ is a stable transfer function. So the rest of the design is to make p as small as possible. Differentiating (12) and noting (7), one obtains

$$M\dot{p} = u + \varphi^T\theta + \tilde{d} \tag{13}$$

where $\dot{x}_{2eq} \triangleq \ddot{y}_d - k_1\dot{e}$ and $\varphi^T = [-\dot{x}_{2eq}, -x_2, -S_f(x_2), -S_r(x_1), 1]$. Noting the structure of (13), the following ARC control law is proposed:

$$u = u_a + u_s, \qquad u_a = -\varphi^T\hat{\theta}, \tag{14}$$

where u_a is the adjustable model compensation needed for achieving perfect tracking, and u_s is a robust control law to be synthesized later. Substituting (14) into (13), and then simplifying the resulting expression, one obtains

$$M\dot{p} = u_s - \varphi^T\tilde{\theta} + \tilde{d}. \tag{15}$$

The robust control law u_s consists of two terms given by:

$$u_s = u_{s1} + u_{s2}, \quad u_{s1} = -k_2 p, \tag{16}$$

where u_{s1} is used to stabilize the nominal system, which is a simple proportional feedback with k_2 being the feedback gain in this case; u_{s2} is a robust feedback used to attenuate the effect of model uncertainties. The same as in [9], there exists a u_{s2} such that the following two conditions are satisfied

$$\begin{aligned} &\text{i} \quad p\{u_{s2} - \varphi^T\tilde{\theta} + \tilde{d}\} \le \varepsilon \\ &\text{ii} \quad pu_{s2} \le 0 \end{aligned} \tag{17}$$

where ε is a design parameter which can be arbitrarily small. Essentially, i of (17) shows that u_{s2} is synthesized to dominate the model uncertainties coming from both parametric

uncertainties $\tilde{\theta}$ and uncertain nonlinearities $\tilde{d}$, and ii of (17) is to make sure that u_{s2} is dissipating in nature so that it does not interfere with the functionality of the adaptive control part u_a. One smooth example of u_{s2} satisfying (17) is given by

$$u_{s2} = -\frac{1}{4\varepsilon}h^2 p. \tag{18}$$

where h is any smoothe function satisfying $h \geq \|\theta_M\|\|\varphi\| + \delta_d$, $\theta_M = \theta_{\max} - \theta_{\min}$.

Theorem 1 *Suppose that the adaptation function in (10) is chosen as $\tau = \varphi p$. Then the ARC control law (14) guarantees:*

A. *In general, all signals are bounded. Furthermore, the positive semi-definite function $V_s = \frac{1}{2}Mp^2$ is bounded by*

$$V_s \leq \exp(-\lambda t)V_s(0) + \frac{\varepsilon}{\lambda}[1 - \exp(-\lambda t)], \tag{19}$$

where $\lambda = 2k_2/\theta_{1\max}$.

B. *If after a finite time t_0, there exist parametric uncertainties only (i.e., $\tilde{d} = 0$, $\forall t \geq t_0$), then, in addition to result A, zero final tracking error is achieved, i.e, $e \to 0$ and $p \to 0$ as $t \to \infty$.*

Proof: The theorem can be proved in the same way as in [5].

4 Desired Compensation ARC (DCARC)

In the ARC design presented in Section 3, the regressor φ in the model compensation u_a (14) and τ depends on states x. Such an adaptation structure may have several potential implementation problems [9]. Firstly, the effect of measurement noise may be severe, and a slow adaptation rate may have to be used, which in turn reduces the effect of parameter adaptation. Secondly, there may exist certain interactions between the model compensation u_a and the robust control u_s, since u_a depends on the actual feedback of the state. This may complicate the controller gain tuning process in implementation. In [13], Sadegh and Horowitz proposed a desired compensation adaptation law, in which the regressor is calculated by desired trajectory information only. The idea was then incorporated in the ARC design in [14, 9]. In the following, the desired compensation ARC is applied on the linear motor system.

The proposed desired compensation ARC law and the adaptation function have the same form as (14) and (10) respectively, but with regressor φ substituted by the desired regressor φ_d:

$$u = u_a + u_s, \quad u_a = -\varphi_d^T\hat{\theta}, \quad \tau = \varphi_d p, \tag{20}$$

where $\varphi_d^T = [-\ddot{y}_d, -\dot{y}_d, -S_f(\dot{y}_d), -S_r(y_d), 1]$. Substituting (20) into (13), and noting $x_2 = \dot{y}_d + \dot{e}$, one obtains

$$\begin{aligned} M\dot{p} &= u_s - \varphi_d^T\tilde{\theta} + (\theta_1 k_1 - \theta_2)\dot{e} + \theta_3[S_f(\dot{y}_d) - S_f(x_2)] \\ &\quad + \theta_{4b}^T[S_r(y_d) - S_r(x_1)] + \tilde{d}. \end{aligned} \tag{21}$$

Comparing (21) with (15), it can be seen that three additional terms appear, which may demand a strengthened robust control function u_s for a robust performance. Applying Mean Value Theorem, it follows that

$$\begin{aligned} S_f(x_2) - S_f(\dot{y}_d) &= g_f(x_2, t)\dot{e}, \\ S_r(x_1) - S_r(y_d) &= g_r(x_1, t)e, \end{aligned} \tag{22}$$

where $g_f(x_2, t)$ and $g_r(x_1, t)$ are nonlinear functions. The strengthened robust control function u_s has the same form as (16):

$$u_s = u_{s1} + u_{s2}, \quad u_{s1} = -k_{s1}p, \tag{23}$$

but with k_{s1} being a nonlinear gain large enough such that the matrix A defined below is positive semi-definite

$$A = \begin{bmatrix} k_{s1} - k_2 - \theta_1 k_1 + \theta_2 + \theta_3 g_f & -\frac{1}{2}(k_1\theta_2 + k_1\theta_3 g_f - \theta_{4b}^T g_r) \\ -\frac{1}{2}(k_1\theta_2 + k_1\theta_3 g_f - \theta_{4b}^T g_r) & \frac{1}{2}Mk_1^3 \end{bmatrix}, \tag{24}$$

and u_{s2} is a required to satisfy the following constrains similar to (17),

$$\begin{aligned} &\text{i} \quad p\{u_{s2} - \varphi_d^T\tilde{\theta} + \tilde{d}\} \leq \varepsilon \\ &\text{ii} \quad pu_{s2} \leq 0 \end{aligned} \tag{25}$$

One smooth example of u_{s2} satisfying (25) is $u_{s2} = -\frac{1}{4\varepsilon}h'^2 p$, where h' is any function satisfying $h' \geq \|\theta_M\|\|\varphi_d\| + \delta_d$.

Remark 1 *It is easy to show that $A \geq 0$, if and only if the following condition is satisfied:*

$$k_{s1} \geq k_2 + \theta_1 k_1 - \theta_2 - \theta_3 g_f + \frac{1}{2\theta_1 k_1^3}(\theta_2 k_1 + \theta_3 k_1 g_f + |\theta_{4b}^T g_r|)^2. \tag{26}$$

Theorem 2 *If the DCARC law (20) is applied, then*

A. *In general, all signals are bounded. Furthermore, the positive definite function V_s defined by*

$$V_s = \frac{1}{2}Mp^2 + \frac{1}{2}Mk_1^2 e^2 \tag{27}$$

is bounded above by

$$V_s \leq \exp(-\lambda t)V_s(0) + \frac{\varepsilon}{\lambda}[1 - \exp(-\lambda t)], \tag{28}$$

where $\lambda = \min\{2k_2/\theta_{1\max}, k_1\}$.

B. *If after a finite time t_0, there exist parametric uncertainties only (i.e., $\tilde{d} = 0$, $\forall t \geq t_0$), then, in addition to result A, zero final tracking error is achieved, i.e, $e \to 0$ and $p \to 0$ as $t \to \infty$.*

Proof: The theorem can be proved in the same way as in [5].

Remark 2 *The motor system is normally equipped with high-resolution position encoder and position measurement feedback is normally quite clean. Comparatively, the velocity measurement is very noisy, which significantly limits the achievable performance. To further alleviate the effect of this noisy velocity feedback, in implementation, the parameter estimates can be updated as follows. Let j represent the sampling instance, ΔT be the sampling period, γ_i be the i-th diagonal element of Γ, $\varphi_{d,i}$ be the i-th component of φ_d and $\Theta_i = \hat{\theta}_i(j\Delta T) + \gamma_i \int_{j\Delta T}^{(j+1)\Delta T} \varphi_{d,i} p \, dt$, then the digital implementation of the continuous adaptation law (10) with τ given by (20) is*

$$\hat{\theta}_i[(j+1)\Delta T] = \begin{cases} \theta_{imax} & \text{if } \Theta_i > \theta_{imax} \\ \theta_{imin} & \text{if } \Theta_i < \theta_{imin} \\ \Theta_i & \text{otherwise} \end{cases} \tag{29}$$

The above digital implementation of parameter estimates needs the feedback of $p = \dot{e} + k_1 e$, which in turn needs the feedback of velocity x_2. Thus, the parameter estimates may be quite noisy if the measurement of the velocity x_2 is noisy. To by-pass this problem, one can rewrite Θ_i as

$$\Theta_i = \hat{\theta}_i(j\Delta T) + \gamma_i \int_{j\Delta T}^{(j+1)\Delta T} \varphi_{d,i}(\dot{e} + k_1 e) \, dt. \tag{30}$$

Since $\varphi_d(t)$ depends on the reference trajectory only and its derivative $\dot{\varphi}_d(t)$ can be pre-computed, one can integrate (30) by parts to obtain,

$$\Theta_i = \hat{\theta}_i(j\Delta T) + \gamma_i(k_1 \int_{j\Delta T}^{(j+1)\Delta T} \varphi_{d,i} e \, dt + \varphi_{d,i} e|_{j\Delta T}^{(j+1)\Delta T} - \int_{j\Delta T}^{(j+1)\Delta T} \dot{\varphi}_{d,i}(t) e \, dt). \quad (31)$$

Thus the parameter estimates implemented through (31) and (29) depend on the desired trajectory and output tracking error only, which are free of velocity measurement noise — another implementation advantage of DCARC. ◇

5 Comparative Experiments

5.1 Experiment Setup

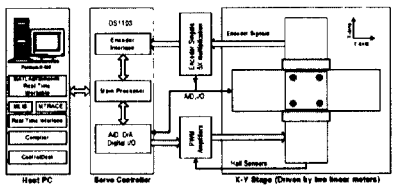

Figure 1: Experimental Setup

To test the proposed nonlinear ARC strategy and study fundamental problems associated with high performance motion control of linear motor drive systems, a two-axis X-Y positioning stage is set up as a test-bed. As shown in Figure 1, the test-bed consists of four major components: a precision X-Y stage with two integrated linear motors, two linear encoders, a servo controller, and a host PC. The two axes of the X-Y stage are mounted orthogonally on a horizontal plane with Y-axis on top of X-axis. A particular feature of the set-up is that the two linear motors are of different type: Y-axis is driven by an Anorad LEM-S-3-S linear motor (epoxy core) and X-axis is driven by an Anorad LCK-S-1 linear motor (iron core). They represent the two most commonly used linear motors and have different characteristics. The resolution of the encoders is 1 μm after quadrature. The velocity signal is obtained by the difference of two consecutive position measurements. In the experiments, only X-axis is used.

Standard least-square identification is performed to obtain the parameters of the X-axis. The nominal value of M is $0.02\ (V/m/s^2)$. To test the learning capability of the proposed DCARC algorithm, we mount a 20 lb load on the motor and the identified values of the parameters are

$$\theta_1 = 0.06\ (V/m/s^2),\ \theta_2 = 0.25\ (V/m/s),\ \theta_3 = 0.06\ (V). \quad (32)$$

Figure 2 shows the force ripple versus the load position for a stroke of 0.4 m. Frequency domain analysis of the measured ripple forces indicates that the fundamental period corresponds to the pitch of the magnets ($P = 60\ mm$) and that the third and fifth harmonics are the main harmonics. Thus the basis functions are chosen as

$$S_r(x_1) = [\sin(\omega x_1), \cos(\omega x_1), \cdots, \sin(5\omega x_1), \cos(5\omega x_1)]^T, \quad (33)$$

where $\omega = 2\pi/P$. The bounds of the parameter variations are thus chosen as:

$$\theta_{\min} = 10^{-2} \cdot [\ 1, 15, 5, -7, -7, -7, -7, -7, -7, -100]^T,$$
$$\theta_{\max} = 10^{-2} \cdot [10, 35, 9,\ 7,\ 7,\ 7,\ 7,\ 7,\ 7,\ 100]^T. \quad (34)$$

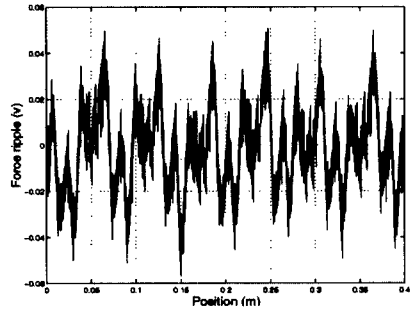

Figure 2: Measurement of force ripple

5.2 Performance Index

As in [14], the following performance indexes will be used to measure the quality of each control algorithm:

- $\|e\|_{rms} = (\frac{1}{T}\int_0^T e(t)^2 dt)^{1/2}$, the *rms value* of the tracking error, is used to measure *average tracking performance*, where T represents the total running time;
- $e_M = \max_t\{|e(t)|\}$, the maximum absolute value of the tracking error, is used to measure *transient performance*;
- $e_F = \max_{T-2\le t\le T}\{|e(t)|\}$, the maximum absolute value of the tracking error during the last 2 seconds, is used to measure *final tracking accuracy*;
- $\|u\|_{rms} = (\frac{1}{T}\int_0^T u(t)^2 dt)^{1/2}$, the average control input, is used to evaluate the amount of *control effort*;
- $c_u = \frac{\|\Delta u\|_{rms}}{\|u\|_{rms}}$, the normalized control variations, is used to measure the *degree of control chattering*, where

$$\|\Delta u\|_{rms} = \sqrt{\frac{1}{N}\sum_{j=1}^{N} |u(j\Delta T) - u((j-1)\Delta T)|^2}\ .$$

is the average of control input increments.

5.3 Comparative Experimental Results

The control system is implemented using a dSPACE DS1103 controller board. The controller executes programs at a sampling frequency $T_s = 0.4\ ms$, which results in a velocity measurement resolution of $0.0025\ m/sec$. In [9], experimental results have shown that DCARC achieves better performance than ARC does in terms of all performance indexes. Thus in this paper, only DCARC algorithm is implemented and the focus is on the comparison of the following three controllers:

PID: PID control with feedforward compensation. Suppose that the parameters of (6) are known, the control objective can be achieved with the following PID control law

$$u = \theta_1 \ddot{y}_d(t) + \theta_2 \dot{y}(t) + \theta_3 S_f(\dot{y}) - K_p e - K_i \int e \, dt - K_d \dot{e}. \quad (35)$$

Closing the loop by applying (35) to (6) easily leads to the closed-loop characteristic equation

$$s^3 + \frac{K_d}{\theta_1} s^2 + \frac{K_p}{\theta_1} s + \frac{K_i}{\theta_1} = 0. \quad (36)$$

By placing the closed-loop poles at desired locations, the design parameters K_p, K_i and K_d can thus be determined. In the experiments, since θ_1, θ_2 and θ_3 are unknown parameters, instead of using (35) the following control law is applied

$$u = \hat{\theta}_1(0)\ddot{y}_d + \hat{\theta}_2(0)\dot{y} + \hat{\theta}_3(0) S_f(\dot{y}) - K_p e - K_i \int e \, dt - K_d \dot{e}, \quad (37)$$

where $\hat{\theta}_1(0)$, $\hat{\theta}_2(0)$ and $\hat{\theta}_3(0)$ are the fixed parameter estimates chosen as 0.05, 0.25 and 0.06, respectively. All the three nominal closed-loop poles are placed at -300 with $K_p = 5.4 \times 10^3$, $K_i = 5.4 \times 10^5$ and $K_d = 18$.

DCARC1 (with force ripple compensation): the controller proposed in section 4. The robust control term u_s in (20) is implemented as follows. Let k_s be a feedback gain large enough such that

$$k_s' = \max\{k_{p1} + \tfrac{1}{4\varepsilon'}h'^2,\ k_{p2} + c(|p| - p_0)^2\} \geq k_{s1} + \tfrac{1}{4\varepsilon'}h'^2, \quad (38)$$

where c and p_0 are two empirical parameters. Then, the control function $u_s = -k_s' p$ satisfies (23) and (25). The parameters of the controller are chosen as: $k_1 = 400$, $k_{p1} = 20$, $k_{p2} = 30$, $\varepsilon' = 10$, $p_0 = 0.02$, $c = 2 \times 10^5$ whenever $|p| > p_0$ and $c = 0$ whenever $|p| \leq p_0$. The continuous function $S_f(x_2)$ is chosen as $\frac{2}{\pi}\arctan(1000x_2)$. The adaptation rates are set as $\Gamma = \mathbf{diag}\{25, 10, 10, 500, 500, 500, 500, 100, 100, 1200\}$. The initial parameter estimates are chosen as: $\hat{\theta}(0) = [0.05, 0.25, 0.06, 0, 0, 0, 0, 0, 0, 0]^T$.

DCARC2 (without force ripple compensation): the same control law as the above DCARC but without force ripple compensation, i.e., $\Gamma = \mathbf{diag}\{25, 10, 10, 0, 0, 0, 0, 0, 0, 1200\}$.

controller	PID	DCARC1	DCARC2
e_M (μm)	131	7.07	8.25
e_F (μm)	7.89	5.18	5.14
$L_2[e]$ (μm)	4.71	1.10	1.47
$L_2[u]$ (V)	0.129	0.121	0.121
$L_2[\Delta u]$ (V)	0.041	0.036	0.036
c_u	0.314	0.299	0.300

Table 1

The motor is first commanded to track a sinusoidal trajectory: $y_r = 0.05sin(4t)$, with a 20lb load mounted on the motor (The inertia is equivalent to $M = 0.06$). The experimental results in terms of performance indexes are given in table 1. As seen from the table, in terms of e_M, e_F and $\|e\|_{rms}$, PID performs poorly, even with a slightly larger degree of control input chattering. One may argue that the performance of PID control can be further improved by increasing the feedback gains. However, in practice, feedback gains have upper limits because the bandwidth of every physical system is finite. To verify this claim, the nominal closed-loop poles of the PID controller are placed at -320 instead of -300, which is easily translated into $K_p = 6144$, $K_i = 655360$ and $K_d = 19.2$. With these gains, the closed-loop system is found to be unstable in experiments. This indicates that the closed-loop bandwidth that a PID controller can achieve in implementation has been pushed almost to its limit and not much further performance improvement can be expected from PID controllers. Thus, in order to realize the high performance potential of the linear motor system, a PID controller even with feedforward compensation may not be sufficient.

In terms of c_u, both DCARC controllers have a better performance than the PID controller. Due to the use of desired compensation structure and the *free-velocity-feedback implementation of parameter adaptation law* presented in Remark 6, DCARC is not so sensitive to velocity measurement noise and thus results in a smaller degree of control chattering.

The tracking errors are given in Figure 3 (the tracking error of the PID controller is chopped off). If the two DCARC controllers are compared, it is seen that DCARC1 performs better in terms of $L_2[e]$, which illustrates the effectiveness of using force ripple compensation. To test the performance robustness of the algorithms to parameter variations, the 20lb payload is removed, which is equivalent to $M = 0.02$. The tracking errors are given in Figure 4. It shows that both DCARC controllers achieve good tracking performance in spite of the change of inertia load.

Then the controllers are test for tracking a fast point-to-point motion trajectory shown in Figure 5. The trajectory has a maximum velocity of $v_{\max} = 1\text{m/s}$ and a maximum acceleration of $a_{\max} = 12\text{m/s}^2$. The tracking errors are shown in Figure 6. As seen, both DCARC controllers achieve much better performance than PID does. Furthermore, during the zero velocity portion of motion, the tracking error is within $\pm 1\mu\text{m}$. It illustrates that, owning to the use of parameter projection mapping, using force ripple compensation in high-speed applications does not affect the stability of the closed-loop system as opposed to the scheme in [4].

Finally, both DCARC controllers are tested for a slow point-to-point motion trajectory similar to the trajectory shown in Figure 5, but with a maximum velocity of $v_{\max} = 0.1\ m/s$ and a maximum acceleration of $a_{\max} = 2\ m/s^2$. The tracking errors are shown in Figure 7. In terms of $L_2[e]$, DCARC1 (0.7 μm) again performs better than DCARC2 (1.0 μm), which further illustrates the effectiveness of force ripple compensation in low-speed applications.

6 Conclusions

In this paper, two ARC controllers have been developed for high performance robust motion control of linear motors. The proposed controller takes into account the effect of model uncertainties coming from the inertia load, friction force, force ripple and external disturbances. In particular, based on the special structure of the ripple forces, design models consisting of known basis functions with unknown weights are used to approximate the unknown nonlinear ripple forces. On-line parameter adaptation is then utilized to reduce the effect of various parametric uncertainties while the uncompensated uncertain nonlinearities are handled effectively via certain robust control laws for high performance. As a result, time-consuming and costly rigorous off-line identification of friction and ripple forces is avoided without sacrificing tracking performance. Experimental results are provided to illustrate the high performance of the proposed schemes.

References

[1] P. V. Braembussche, J. Swevers, H. V. Brussel, and P. Vanherck, "Accurate Tracking control of Linear Synchronous Motor Machine tool Axes," *Mechatronics*, vol. 6, no. 5, pp. 507-521, 1996.

[2] D. M. Alter and T. C. Tsao, "Control of linear motors for machine tool feed drives: design and implementation of h_∞ optimal feedback control," *ASME J. of Dynamic systems, Measurement, and Control*, vol. 118, pp. 649-656, 1996.

[3] T. Egami and T. Tsuchiya, "Disturbance Suppression Control with Preview Action of Linear DC Brushless Motor," *IEEE Transactions on Industrial Electronics*, vol. 42, no. 5, pp. 494–500, 1995.

[4] G. Otten, T. Vries, J. Amerongen, A. Rankers, and E. Gaal, "Linear Motor Motion Control Using a Learning Feedforward Controller," *IEEE/ASME Transactions on Mechatronics*, vol. 2, no. 3, pp. 179–187, 1997.

[5] B. Yao and L. Xu, "Adaptive robust control of linear motors for precision manufacturing," in *The 14th IFAC World Congress, Vol. A*, pp. 25–30, 1999.

[6] S. Komada, M. Ishida, K. Ohnishi, and T. Hori, "Disturbance Observer-Based Motion Control of Direct Drive Motors," *IEEE Transactions on Energy Conversion*, vol. 6, no. 3, pp. 553–559, 1991.

[7] B. Yao and M. Tomizuka, "Smooth robust adaptive sliding mode control of robot manipulators with guaranteed transient performance," *Trans. of ASME, Journal of Dynamic Systems, Measurement and Control*, vol. 118, no. 4, pp. 764–775, 1996.

[8] B. Yao and M. Tomizuka, "Adaptive robust control of SISO nonlinear systems in a semi-strict feedback form," *Automatica*, vol. 33, no. 5, pp. 893–900, 1997.

[9] L. Xu and B. Yao, "Adaptive robust precision motion control of linear motors with negligible electrical dynamics: theory and experiments," in *Proc. of American Control Conference*, 2000.

[10] J. Y. Hung and Z. Ding, "Design of currents to reduce torque ripple in brushless permanent magnet motors," *Proc. Inst. Elect. Elect. Eng.*, vol. 140, no. 4, pp. 260–266, 1993.

[11] B. Armstrong-Hélouvry, P. Dupont, and C. Canudas de Wit, "A survey of models, analysis tools and compensation methods for the control of machines with friction," *Automatica*, vol. 30, no. 7, pp. 1083–1138, 1994.

[12] S. Sastry and M. Bodson, *Adaptive Control: Stability, Convergence and Robustness*. Englewood Cliffs, NJ 07632, USA: Prentice Hall, Inc., 1989.

[13] N. Sadegh and R. Horowitz, "Stability and robustness analysis of a class of adaptive controllers for robot manipulators," *Int. J. Robotic Research*, vol. 9, no. 3, pp. 74–92, 1990.

[14] B. Yao and M. Tomizuka, "Comparative experiments of robust and adaptive control with new robust adaptive controllers for robot manipulators," in *Proc. of IEEE Conf. on Decision and Control*, pp. 1290–1295, 1994.

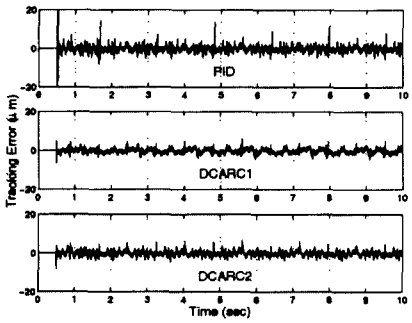

Figure 3: Tracking errors for sinusoidal trajectory with load

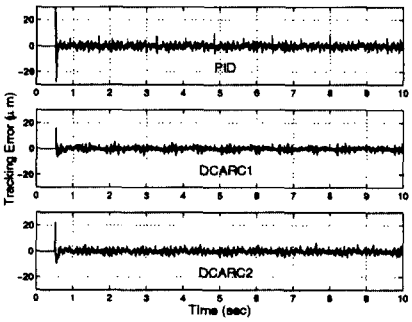

Figure 4: Tracking errors for sinusoidal trajectory without load

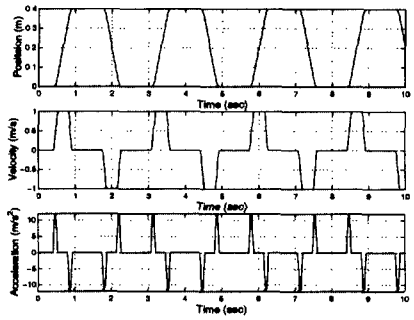

Figure 5: High-acceleration/high-speed point-to-point motion trajectory

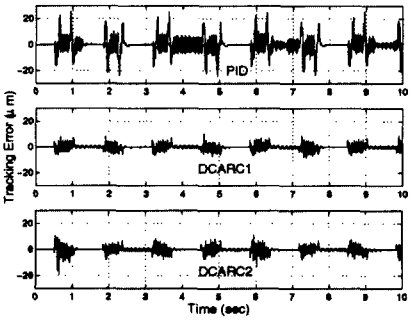

Figure 6: Tracking errors for high-acceleration/high-speed point-to-point motion trajectory

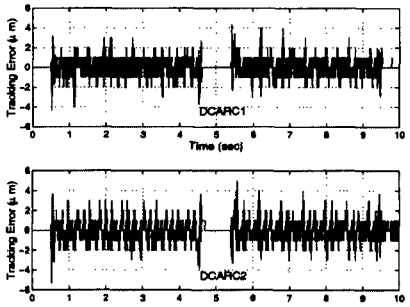

Figure 7: Tracking errors for low-speed point-to-point motion trajectory